The Wettzell Ring Laser “G” as a North-South Tilt Probe

MENDES CERVEIRA Paulo Jorge[1]

1) BEWAG Geoservice GmbH, Thomas Alva Edison-Straße 1, A-7000 Eisenstadt
paulo.mendes@geoservice.at

Summary : The ring laser “G” located in Wettzell, Germany, is a north-south tilt probe for periods between one hour and two days, after removing all nuisance components, especially the part arising due to Earth orientation variations. In contrast to high-sensitive tiltmeters, the ring laser does only sense tilts induced by deformation (no attraction), and is therefore a function of the potential Love and Shida numbers h_2 and l_2, while tiltmeters do include the Love number k_2. The optimum Love numbers, derived from the “G” ring laser and the nearby tiltmeter, are $h_2 = 0.6573$, and $k_2 = 0.3577$. This result is obtained for a fixed nominal value $l_2 = 0.0847$.

1. Introduction

In principle, deformations of the Earth’s surface induce changes in the local vertical. A lunar signal has been predicted for large ring laser gyroscopes [Rautenberg et al., 1997], and this has been detected recently for the first time for the C-II ring laser, located in Cashmere, Christchurch, New Zealand [Schreiber et al., 2003]. In the last years, a new prototype, the “G” ring laser in Wettzell, Germany, has proven highest accuracy and resolution in detecting signatures in Earth orientation [Schreiber et al., 2004].

2. The Wettzell ring laser “G” and the Sagnac frequency

The Wettzell ring laser “G” (see figure 1) is a sensor using the Sagnac effect [Anderson et al., 1994] and being in operation since the year 2001 [Schreiber et al., 2008]. Its size is 4m x 4m consisting basically of the glass ceramic Zerodur due to the extreme mechanical and thermal stability that is required. It is located in an underground laboratory operating in stable thermal conditions. The main functioning is as follows: two counter-rotating laser beams are splitted by frequency if a rotation occurs. In such a case a beat frequency can be observed, and is called Sagnac frequency f . This beat frequency is inverse proportional to the perimeter of the beam path length P and the optical wavelength λ, and proportional to the enclosed area A, the normal vector $\boldsymbol{n}$ to A, and finally to the instantaneous rotation vector $\boldsymbol{\Omega}$ of the Earth [Schreiber et al., 2003]:

$$f = \frac{4 \cdot A}{\lambda \cdot P} \cdot \boldsymbol{n}^T \cdot \boldsymbol{\Omega} \qquad (1)$$

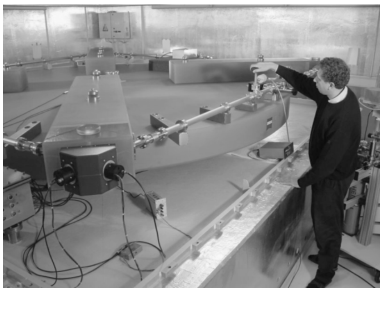

Figure 1 The Wettzell “G” ring laser adjusted by Prof. Schreiber.

3. The rotational perturbation in the relative Sagnac frequency

3.1 Earth orientation data and models

Earth orientation is commonly described by 5 parameters, two associated with the motion of the Celestial Intermediate Pole (CIP) in space, one for the Earth's angle of spin and two for the terrestrial motion of the CIP [Capitaine et al., 2002], see figure 2. And, this description is quite practical. However, such a parameterization requires a conventional distinction between high-frequency polar motion and nutation: precession-nutation is the terrestrial retrograde motion of the CIP with frequencies between one cycle in 48 hours and one cycle in 16 hours (sidereal), while all other motions of the CIP are interpreted as polar motion. Let $\mathbf{M}$ be the matrix for the coordinate transformation from the ITRS (International Terrestrial Reference System) to the GCRS (Geocentric Celestial Reference System). The realized CIP is defined through the computed equatorial components, X and Y, of the mean geographic axis in the GCRS by the IAU2000 precession-nutation model. The offset between this computed position of the CIP and the estimated one is called "celestial pole offset", with the components $\delta\mathrm{X}$ and $\delta\mathrm{Y}$. The equatorial position of the CIP in space is therefore composed of the computed CIP plus the celestial pole offset, and of the complementary terms, which are usually provided w.r.t. the ITRS. The latter are the terrestrial coordinates $\mathrm{p} = \mathrm{x} - \mathrm{i} \cdot \mathrm{y}$ of the CIP. The adopted transformation matrix $\mathbf{M}$, referred to the non-rotating origin, is given by:

$$\mathbf{M} = \mathbf{PN}(\mathrm{X} + \delta\mathrm{X}, \mathrm{Y} + \delta\mathrm{Y}) \cdot \mathbf{R}(\Omega \cdot \mathrm{UT1}) \cdot \mathbf{W}(\mathrm{x}, \mathrm{y}) \tag{2}$$

where $\mathbf{PN}$ is related with the precession-nutation model and the celestial pole offsets, $\mathbf{R}$ to the angle of rotation around the CIP and $\mathbf{W}$ to the terrestrial position of the CIP.

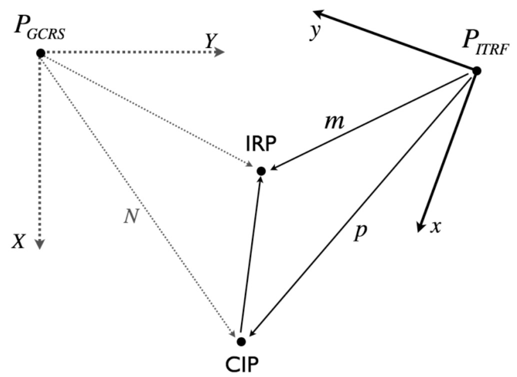

Figure 2 Celestial Intermediate Pole (CIP) versus Instantaneous Rotation Pole (IRP). Precession-nutation of the CIP is denoted by *N*.

Through the International Earth Rotation and Reference systems Service (IERS), the daily corrections $(\delta\mathrm{X}, \delta\mathrm{Y})$, UT1-UTC and (x, y) are available (EOPC04 05). We note that the zonal tidal terms are already included in the UT1-UTC time series. Then, the five parameters of each series are interpolated by using cubic spline functions at 30-minutes intervals. Our investigation is restricted to the time span from September 22$^{\mathrm{nd}}$ 2006 (MJD 54000) to February 13$^{\mathrm{th}}$ 2007 (MJD 54144).

In addition, we have taken into consideration diurnal and subdiurnal signatures. The diurnal (prograde) and semi-diurnal (pro- and retrograde) effect of ocean tides (71 tidal constituents) has to be computed, at 30 minutes intervals, for both the Earth rotation angle UT1 and the polar motion ($\mathrm{p} = \mathrm{x} - \mathrm{i} \cdot \mathrm{y}$) of the CIP [IERS Conventions, 2004]. Moreover, retrograde diurnal (nutation) terms due to tidal gravitation (lunisolar) need to be computed for the polar motion of the CIP. So far, no official model is available for the effect of Earth's multipole structure upon its rotation angle. However, the model of [Wünsch, 1991] has been applied, as this effect may reach up to 3 µs in UT1.

3.2 Transformation to the instantaneous Earth rotation vector

The components of the instantaneous rotation vector (at a temporal resolution of 30 minutes) are directly calculated from the product of the matrices $\dot{\mathbf{M}}$ and $\mathbf{M}^{\mathbf{T}}$. In the terrestrial frame, we have:

$$\mathbf{M}^{\mathbf{T}} \cdot \dot{\mathbf{M}} = \begin{bmatrix} 0 & -\Omega_z & \Omega_y \\ \Omega_z & 0 & -\Omega_x \\ -\Omega_y & \Omega_x & 0 \end{bmatrix} \tag{3}$$

The terrestrial coordinates of the instantaneous pole of rotation (IRP) are defined through:

$$\vec{\Omega} = \begin{pmatrix} \Omega_x \\ \Omega_y \\ \Omega_z \end{pmatrix} = \Omega_0 \cdot \begin{pmatrix} m_x \\ m_y \\ 1 + m_z \end{pmatrix} \tag{4}$$

The decortication of the motion of the IRP into its various components has been developed in the last decades in great detail, e.g., [Brzezinski, 1986; Gross, 1992; Brzezinski and Capitaine, 1993].

The determination of high frequency variations of the IRP from VLBI data is described in a clear fashion by [Bolotin et al., 1997]. The use of the instantaneous Earth rotation vector in the reduction of superconducting gravimetry observations has been applied first by [Loyer et al., 1999].

3.3 Transformation to the relative Sagnac frequency

The relative Sagnac frequency is defined as:

$$\Delta f = \frac{f - f_0}{f_0} \tag{5}$$

where f_0 is the nominal Sagnac frequency for the ring laser "G" at Wettzell. If we assume that the perimeter of the beam path length P, the optical wavelength λ, and the enclosed area A are highly stable, then the relative Sagnac frequency is given to first order by [Mendes Cerveira et al., 2008]:

$$\begin{aligned} \Delta f &\approx \frac{\Delta \boldsymbol{n}^T \cdot \boldsymbol{\Omega}_0 + \boldsymbol{n}_0^T \cdot \Delta \boldsymbol{\Omega}}{\boldsymbol{n}_0^T \cdot \boldsymbol{\Omega}_0} \\ &\approx \cot \varphi_0 \cdot \left[m_x \cdot \cos \lambda_0 + m_y \cdot \sin \lambda_0 + \Delta \varphi_{top} \right] + m_z \end{aligned} \tag{6}$$

where φ_0 and λ_0 are the nominal latitude and longitude of the ring laser "G", $\Delta\varphi_{top}$ is the topocentric latitudinal deflection (tilt), $\boldsymbol{\Omega}_0$ is the nominal Earth rotation vector, $\Delta\boldsymbol{\Omega}$ its perturbation, and $\boldsymbol{n}_0$ is the nominal unitary normal vector and $\Delta\boldsymbol{n}$ its perturbation. The component m_z is directly related to the excess length of day (LOD) [Gross, 2007]. Figure 3 classifies the relative Sagnac frequency variation due to Earth orientation changes into its sub-components.

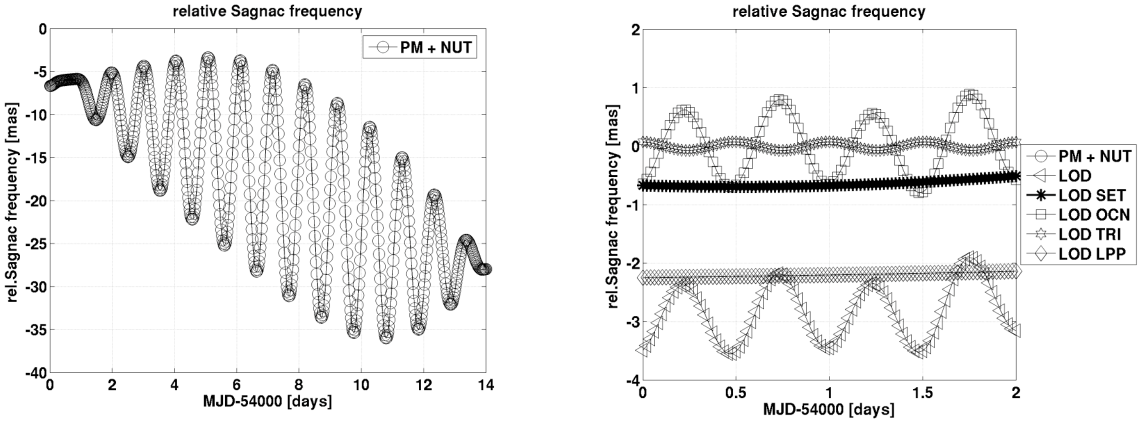

Figure 3 Computed relative Sagnac frequency variation from Earth orientation data and models in units of milliarcseconds (mas), from MJD 54000 to 54144. It is shown (*left panel*) for polar motion and precession-nutation (PM +NUT), (*right panel*) for LOD (total), for the solid Earth tides (LOD SET), for the ocean tides (LOD OCN), for the triaxiality (LOD TRI), and for the long period part (LOD LPP). The latter is mainly due to atmosphere angular momentum exchange.

4. Deformations due to exogenic and endogenic causes

Local effects are an important limitation in the accuracy of ring laser observables. Especially in the context of space geodesy, the study of such effects is of increasing importance. As the ring laser is coupled to the local Earth's surface, it is sensitive to deformations induced by exogenic and endogenic causes. Endogenic deformations are usually small or episodic in time and local in space (e.g. earthquakes). Exogenic deformations arise due to tidal forces and surface loading and traction (e.g. Earth body tides or tidal and non-tidal oceanic, atmospheric and hydrological loading) [Rautenberg et al., 1997].

The computation of the effect of the solid Earth tides in the relative Sagnac frequency is based on the model of [Mathews et al., 2002]. This model provides latitudinal displacements, which can be converted, through the Love numbers formalism, into latitudinal deflections, which are then transformed to the relative Sagnac frequency by equation 6.

5. Data analysis and results

5.1 Tiltmeter data

The tilmeter data (in north-south direction) was obtained for the time span September 22nd, 2006 to February 13th, 2007 with a temporal resolution of 30 minutes. Most of the signal seen in the tiltmeter data of Wettzell (see figure 4, left panel) contains the effect of the solid Earth tides, which has been derived from a model for north-south displacements [Mathews et al., 1997]. After removal of the tilt induced by the solid Earth tides, the effect of the ocean tides remain (see figure 4, right panel). The spectral amplitude and standard deviation (std) of the residuals has been obtained from forming a scalogram and averaging over the period band. The long-period part (larger than 2 days) has been filtered out after removing all known (modelled) signals.

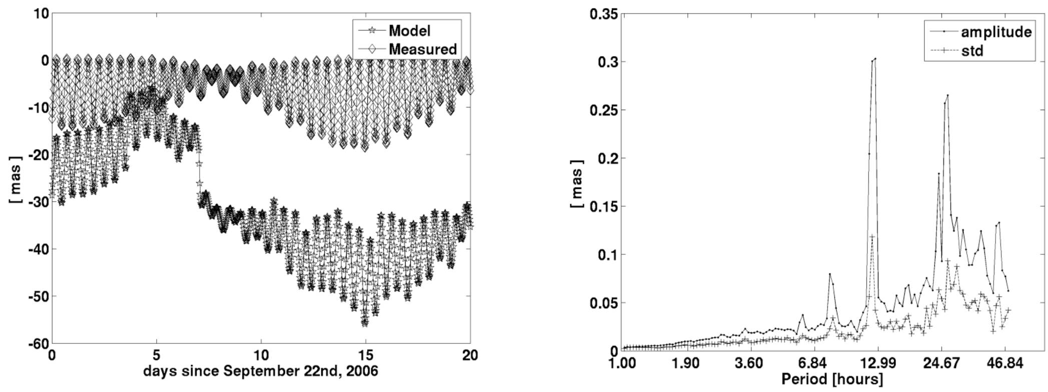

Figure 4 Computed (solid Earth tides model) and measured tilt in units of mas, from MJD 54000 to 54144. Only the 20 first days are shown for better visibility (*left panel*). The amplitude spectrum of the residual tiltmeter series (measured minus effect of solid Earth tides) is shown for periods between one and 48 hours (*right panel*). Sharp spectral peaks occur at 6, 8, 12, 24 and 25.8 hours in the residual tiltmeter series, and are mostly of ocean tidal origin.

5.2 Ring laser data

The ring laser data (relative Sagnac frequency) was also measured for the time span September 22nd, 2006 to February 13th, 2007 again with a temporal resolution of 30 minutes.

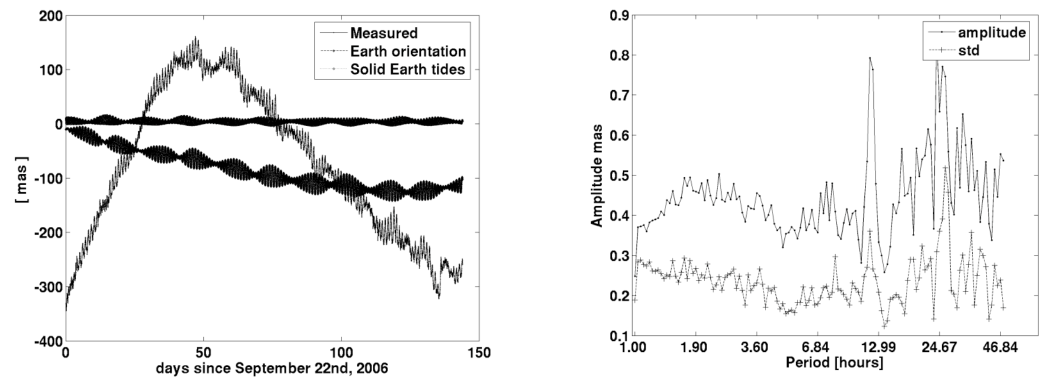

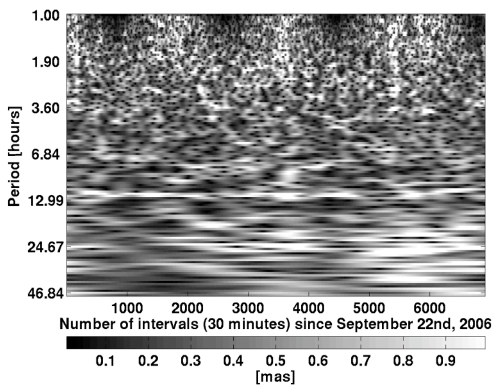

Figure 5 Computed (Earth orientation and solid Earth tides) and measured relative Sagnac frequency in units of mas, from MJD 54000 to 54144. The amplitude spectrum of the residual ring laser time series (measured minus effect of Earth orientation and solid Earth tides) is shown for periods between one and 48 hours. Residual spectral peaks occur at 12 (S2 wave) and 25.8 (O1 wave) hours and are still of unknown origin. The standard deviation in the O1 wave is of the level of 0.5 mas, while the one for the S2 wave is only 0.3 mas

Figure 5 (top left panel) shows the largest contributions to the relative Sagnac frequency variation, i.e., the Earth orientation variation and the effect of the solid Earth tides upon the local vertical. The top right panel (derived again from the scalogram, shown at the bottom left panel) brings to evidence a clear spectral peak, in the residual ring laser time series (measured minus Earth orientation minus solid Earth tides), for the S2 wave. Here, signals larger than two days have been filtered out. Besides, a regular increase in noise with a period of about one month can be detected in the scalogram (between one and three hours).

6. Love numbers and tilt factor

A north-south displacement d_{NS} of tidal origin is related through the tidal potential $V_n(r,\varphi,\lambda)$ by [Lambotte et al., 2006]:

$$d_{NS}(r,\varphi,\lambda) = \frac{l_n(r)}{g(r)} \cdot \frac{\partial V_n(r,\varphi,\lambda)}{\partial \varphi} \tag{7}$$

The north-south tilt sensed by a ring laser (only sensitive to deformation) is related through the tidal potential by:

$$t_{NS,RLG}(r,\varphi,\lambda) = \cot\varphi_0 \cdot \frac{\gamma_n(r)}{r \cdot g(r)} \cdot \frac{\partial V_n(r,\varphi,\lambda)}{\partial \varphi} \tag{8}$$

with the tilt factor $\gamma_n(r) = -h_n(r)$. Contrary to a ring laser, a tiltmeter also reacts to the induced attraction of the deformed Earth. For this reason, the tilt factor to which a tiltmeter is sensitive has the form $\gamma_n(r) = 1 + k_n(r) - h_n(r)$.

Therefore, the ratio of the degree-2 Love and Shida numbers (for an SNREI Earth model) when using the ring laser is given by:

$$\frac{h_2}{l_2} = -\frac{r \cdot t_{NS,RLG}}{\cot\varphi_0 \cdot d_{NS}} \tag{9}$$

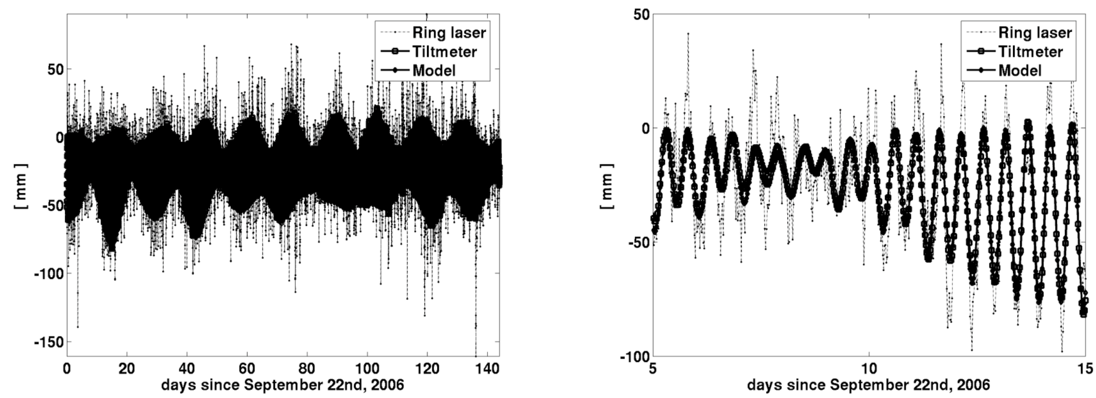

Figure 6 Measured (ring laser and tiltmeter) and modelled north-south displacement in units of mm, from MJD 54000 to 54144. The plot on the right shows a zoom for ten days since September 27th, 2006.

Figure 6 shows the north-south displacements in units of mm, derived from the ring laser data, the tiltmeter data, and a model [Mathews et al., 1997].

The respective factors, containing the Love numbers, have been varied from 0.5 to 1.5 w.r.t. to the nominal ones (for ring laser and tiltmeter), in order to minimize the standard deviation of the residuals (ring laser minus model, and tiltmeter minus model, see figure 7). If we consider the nominal Shida number $l_2 = 0.0847$ to be stable, we find optimal Love numbers: $h_2 = 0.6573$ and $k_2 = 0.3577$ (see figure 7).

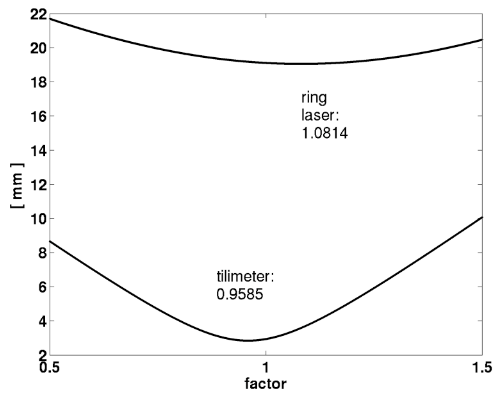

Figure 7 Minima for standard deviation of residuals (w.r.t. the model displacement in north-south direction) in units of mm. For the ring laser we obtain an optimum factor of 1.0814, while the optimum factor is 0.9585 for the tiltmeter. The minimum standard deviation for the ring laser is 19.1 mm, while the one for the tiltmeter is 2.9 mm.

7. Conclusions

At regular intervals of about one month, the noise of the "G" ring laser is considerably increased (~1 mas) in the frequency domain between one and three hours. The source of this noise is, for the moment being, unknown.

The ring laser "G" is able to monitor local tilts induced by local deformation. Although its sensitivity is one order of magnitude lower than that of the best tiltmeters, it was possible to estimate optimum Love numbers of degree 2, given a known nominal Shida number.

Acknowledgments

The author is very grateful to Dr. Thomas Klügel (BKG) and Prof. U. Schreiber (FESG) for providing access to the ring laser and tiltmeter data. I thank Prof. Bernard Ducarme for reviewing this manuscript and detecting a typo in formula (9).

References

1. Anderson R., H.R. Bilger and G.E. Stedman, *"Sagnac" effect: A century of Earth-rotated interferometers*, Am. J. Phys., Vol. 62 (11), pp. 975-985 (**1994**)
2. Bolotin S., C. Bizouard, S. Loyer and N. Capitaine*, High frequency variations of the Earth's instantaneous angular velocity vector. Determination from VLBI data analysis*, Astronomy and Astrophysics, Vol. 317, pp. 601-609 (**1997**)
3. Brzezinski A., *Contribution to the theory of polar motion for an elastic earth with liquid core*, manuscripta geodaetica, Vol. 11, pp. 226-241 (**1986**)
4. Brzezinski A. and N. Capitaine, *The use of the precise observations of the Celestial Ephemeris Pole in the analysis of geophysical excitation of Earth rotation*, J. Geophys. Res., Vol. 98 (B4), pp. 6667-6675 (**1993**)
5. Capitaine N., D. Gambis, D. McCarthy, G. Petit, J. Ray, B. Richter, M. Rothacher, M. Standish and J. Vondrak, Proceedings of the IERS Workshop on the Implementation of the New IAU Resolutions, *IERS Technical Note No. 29*, Frankfurt am Main: Verlag des Bundesamts für Kartographie und Geodäsie (**2002**)
6. Gross R.S., *Correspondence between theory and observations of polar motion*, Geophys. J. Int., Vol. 109, pp. 162-170 (**1992**)
7. Gross R.S., *Earth Rotation Variations – Long Period*, in Physical geodesy, T.A. Herring (ed.), pp. 239-294, Treatise on Geophysics, Vol. 3, Elsevier, Oxford (**2007**)
8. IERS Conventions (2003), Chapter 8: *Tidal Variations in the Earth's Rotation*, editors: McCarthy D.D. and G. Petit, IERS Technical Note 32, Frankfurt am Main: Verlag des Bundesamts für Kartographie und Geodäsie, 2004, paperback, ISBN 3-89888-884-3 (**2004**)
9. Lambotte S., L. Rivera and J. Hinderer, Vertical and horizontal seismometric observations of tides, Journal of Geodynamics, Vol. 41, pp. 39 – 58 (**2006**)
10. Loyer S., J. Hinderer and J.-P. Boy, *Determination of the gravimetric factor at the Chandler period from Earth orientation data and superconducting gravimetry observations*, Geophysical Journal International, Vol. 136 (1), pp. 1-7 (**1999**)
11. Mathews P.M., V. Dehant and J.M. Gipson, *Tidal station displacements*, J. Geophys. Res., Vol. 102 (B9), pp.

20469 – 20477 (**1997**)
12. Mathews P.M., T.A. Herring and B.A. Buffet, *Modeling of nutation and precession: new nutation series for nonrigid Earth and insights into the Earth's interior*, J. Geophys. Res., Vol. 107 (B4), doi: 10.1029/2001JB000390 (**2002**)
13. Mendes Cerveira P.J., H. Spicakova, H. Schuh, T. Klügel, U. Schreiber and A. Velikoseltsev, *Earth rotation parameters from Very Long Baseline Interferometry and ring laser observables*, accepted for Advances in Geosciences (**2008**)
14. Rautenberg V., H.P. Plag, M. Burns, G.E. Stedman and H.U. Jüttner, *Tidally induced Sagnac signal in a ring laser*, Geophys. Res. Lett., Vol. 24 (8), pp. 893-896 (**1997**)
15. Schreiber K.U., T. Klügel and G.E. Stedman, *Earth tide and tilt detection by a ring laser gyroscope*, J. Geophys. Res., Vol. 108 (B2), doi: 10.1029/2001JB000569 (**2003**)
16. Schreiber K.U., A. Velikoseltsev, M. Rothacher, T. Klügel and G.E. Stedman, *Direct measurement of diurnal polar motion by ring laser gyroscopes*, J. Geophys. Res., Vol. 109 (B06405), doi: 10.1029/2003JB002803 (**2004**)
17. Schreiber K.U., T. Klügel, A. Velikoseltsev, W. Schlüter and G.E. Stedman, *The Large ring laser G for Continuous Earth Rotation Monitoring*, submitted to Pure and Applied Geophysics (**2008**)
18. Wünsch J., *Small waves in UT1 caused by the inequality of the equatorial moments of inertia A and B of the Earth*, Astron. Nachr., Vol. 312, 5, pp. 321 – 325 (**1991**)